

Design, Modeling, and Control of Norma: a Slider & Pendulum-Driven Spherical Robot

Saeed Moazami¹, M-Mahdi Naddaf-Sh¹, Srinivas Palanki², and Hassan Zargarzadeh¹

ABSTRACT

This paper discusses the design, modeling, and control of Norma, a novel 2-DOF mobile spherical robot (SR). The propelling mechanism of this robot consists of two actuators: a slider, and a rotational pendulum located on the SR's diagonal shaft. The slider can translate along the shaft and shift the robot's center of gravity towards the robot's sides. The pendulum rotates around the shaft to propel the SR to roll forward and backward. These two actuators enable the SR to perform both rolling and turning maneuvers as a nonholonomic robot. The advantage of the proposed mechanical design lies in its convenience of physical implementation, agility, and accurate mathematical model. The Euler-Lagrange approach is utilized to derive dynamics of the proposed mechanical structure using minimum simplifications possible. Further, a path tracking control scheme is introduced for a smooth trajectory. Finally, simulations are carried out in MATLAB to verify the accuracy of the mathematical model and the effectiveness of the controller against experimental results.

Keywords:

Spherical Robot, Euler-Lagrange, Mathematical Modeling, Dynamics, Mobile Robot.

1. INTRODUCTION

Spherical robots (SRs) are a class of mobile robots that are generally identified by their ball-shaped shell and internal electro-mechanical driving components that provide torques required for their rolling motion [1-4]. Despite their limitations, due to their ball-shaped exterior, SRs inherit multiple advantages over other types of mobile robots where skidding, tipping over, falling, or friction with the surface makes them vulnerable or inefficient. Furthermore, incorporating particular considerations into the design of SRs, all internal components of the robot can be protected from collision and environmental states such as moisture, radiation, dust etc. These unique features make SRs a suitable candidate for various applications such as surveillance [5], environmental monitoring [6], exploration operations in unknown environments [7], agriculture [8], rehabilitation [9], and hobbies [10]. Nonetheless, compared to other types of mobile robots, e.g., wheeled and legged robots, SRs are by far underemphasized by researchers in the field of mobile robotics. One reason can be the complicated, nonlinear and usually nonholonomic dynamics of SRs that has remained a hurdle to fully comprehend their behavior and maneuverability features.

There are a number of SR classifications available in the literature. In [1], SRs are classified based on their mechanical configurations, e.g., wheeled [11], pendulum driven [12-16], gimbal mechanism [17], single ball [1], mass movement [18], and a set of designs that use flywheels [19, 20]. SRs can also be classified based on their kinematics behavior [4] into Continuous Rolling Spherical Robots (CR-SR), and Rolling and

¹ Phillip M. Drayer Department of Electrical Engineering at Lamar University, Beaumont, TX, USA. (e-mails: smozami@lamar.edu, mnaddafsharg@lamar.edu, h.zargar@lamar.edu).

² Dan F. Smith Department of Chemical Engineering at Lamar University, Beaumont, TX, USA. (e-mail: spalanki@lamar.edu).

Steering Spherical Robots (RS-SR). Alternatively, in [2], SRs are classified based on their mechanical driving principles as: 1) conservation of angular momentum (COAM), in which SRs utilize flywheels to provide propelling torques, 2) outer shell transformation (OST), that the robots deform different parts of their outer shell in order to propel themselves, and 3) barycenter offset (BCO), where SRs shift their center of gravity to provide gravitational torque. It can be noted that a majority of SRs developed by the researchers belong to BCO SRs and one of the most popular structures in this class is pendulum-driven spherical robot (PDSR).

PDSRs are usually modeled as a spherical shell with a diagonal shaft and a pendulum mounted on the shaft, rotating about the shaft's axis. In the literature, several mechanisms of PDSRs have been proposed that utilize either a single 2-DOF pendulum [21-24], or double-pendulum structure [25-27] as the source of gravitational torque. In [28], mathematical model of a PDSR is derived using a decoupled dynamics approach. From a different view, the model of a PDSR is studied in [29, 30], where the desired path is assumed to be a straight line with constant slope and a 2D curved path with variable-slope respectively. Likewise, in [31], the mathematical model is derived for a SR using Lagrangian reduction theory defined on symmetry groups. Authors in [13], have extensively investigated the dynamics and control problem of a SR, while the primary focus of the paper is less on the practical aspects of the robot.

Taking a step forward, with the aim to introduce a novel SR model, this paper investigates the modeling and control of Norma, a lab-made SR with a 2-DOF propelling mechanism which is comprised of a linear and a rotational actuator located on a diagonal shaft fixed to a solid spherical shell. The rotational actuator provides gravitational torque for rolling action of the SR along the longitudinal direction by applying torque through a pendulum to the shaft. The linear actuator translates a sliding weight on the shaft that shifts the center of gravity of the robot in the transverse direction causing the robot to tilt and consequently providing the turning maneuverability for the robot. To derive the mathematical model of Norma, first, a conceptual model is presented that is remarkably close to its mechanical structure. Then, Euler-Lagrange method is utilized to derive the dynamics of the proposed SR where minimum possible simplifying assumptions are made.

The path tracking control of SRs has been a challenge due to its nonholonomic and underactuated features. In this paper, this problem is addressed by a control scheme that decouples the SR's kinematics from its dynamics. To that end, first, a set of PID controllers are designed that stabilize the SR's rolling angular velocity, $\dot{\theta}$, and its slider displacement, δ , around and along the transverse axis respectively. Then, a path planning algorithm is devised that governs $\dot{\theta}$ and δ based on the path tracking error and the robot's physical constraints. Finally, numerical and laboratory experiments are carried out to evaluate the SR model's accuracy and the controller's tracking performance. The conducted experiments show that the controller can control both the numerical model in MATLAB, and the actual robot.

The rest of the paper is organized into the following sections: the description of the proposed model is given in the second section; in the third section, kinematics and dynamics models are developed; in section four, the control scheme is presented. The simulation and experimental results are represented in section five, followed by the conclusions in the last section.

2. MODEL DESCRIPTION

Fig. 1 illustrates the mechanical schematic diagram of the proposed SR. The robot consists of a ball-shaped rigid shell, a diagonal shaft, a linear, and a rotational actuator. The shaft is along the transverse axis of the sphere, and it is fixed to the shell. To provide the rolling motion, the pendulum can apply torque \mathcal{T} to the shaft around the transverse axis using Motor-1. This torque causes the sphere to roll forward and backward

along the longitudinal axis which is horizontal and perpendicular to the transverse axis. The slider translates along the shaft's axis using force \mathcal{F} applied by the linear Motor-2. Translation of the slider shifts the center of mass of the spherical robot in the transverse direction, resulting in the shaft and the sphere to tilt about the longitudinal axis. So, the proposed SR has the ability of both rolling towards the longitudinal axis and tilting about the same axis enabling it to have a nonholonomic motion.

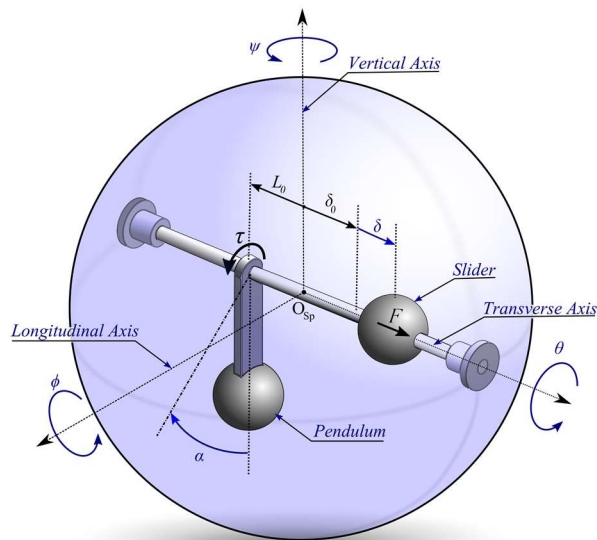


Fig. 1. Schematic diagram of Norma, the proposed SR.

Fig. 2 shows the mechanical configuration of the laboratory fabricated model of the robot named Norma, Latin root of the word “Normal”. The reason for choosing this name is the configuration of the robot, where the axis of the motion of the slider is normal to the pendulum.

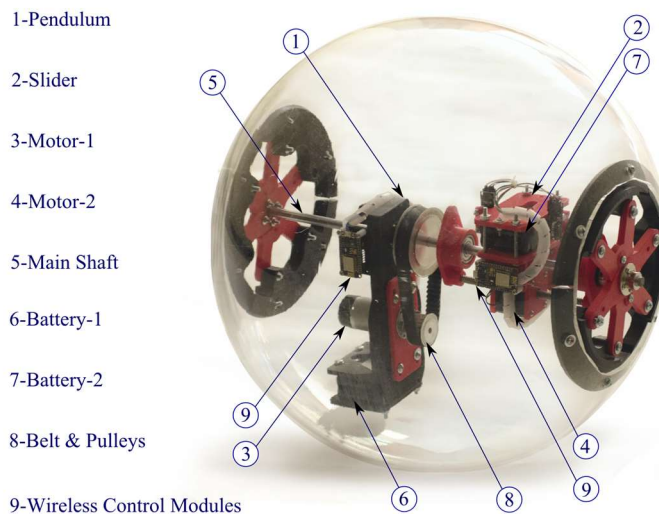


Fig. 2. Mechanical structure of Norma.

Assumptions: with no loss of generality, the following assumptions are made for deriving the kinematics and dynamics of the SR:

- 1) *The sphere rolls over a perfectly flat horizontal plane surface without slipping.*
- 2) *The slider and pendulum bob are point masses and the pendulum rod is massless.*

When motors apply no force and torque, the SR is designed to have a resting static equilibrium point

(RSEP) where the pendulum rod is perpendicular to the ground and the transverse axis is horizontal. At this point, the plumb line from the sphere center, denoted as O_{sp} , passes through the robot's center of gravity. Considering m_p , L_0 , m_{sl} , δ_0 respectively as the pendulum's mass, distance of the pendulum's point of suspension from O_{sp} , slider mass, and the slider's distance from O_{sp} at RSEP, we can write:

$$m_p L_0 = m_{sl} \delta_0. \quad (1)$$

The next step is to define the SR generalized coordinates. As shown in Fig. 1, θ and ϕ are the rotation angles of the sphere about the transverse and longitudinal axes respectively. In fact, ϕ is the tilting angle of the sphere. Propelled by Motor-1, α is the rotation of the pendulum about the shaft which is in the opposite direction to θ . Also, propelled by Motor-2, δ is the displacement of the slider along the shaft axis with respect to δ_0 as the origin.

In the sequel, reference frames are denoted as $\{\mathcal{F}\}$, where \mathcal{F} is the set of frame axes. The reference frame of any vector quantity is shown in its left superscript e.g., ${}^{\mathcal{F}}A$ represents A in $\{\mathcal{F}\}$. Rotation matrices are denoted as $\mathcal{R}_{\mathcal{F}_B \mathcal{F}_A}$ which transforms vectors from $\{\mathcal{F}_A\}$ to $\{\mathcal{F}_B\}$.

Fig. 3 illustrates the reference frames that are used to derive the equations of motion of the spherical robot. $\{\mathcal{F}_w\}$ with axes $\{X_w^-, Y_w^-, Z_w^-\}$ is the world coordinate frame fixed to the ground at its origin O_w . Position coordinates of the SR in $\{\mathcal{F}_w\}$ are denoted as:

$${}^{\mathcal{F}_w} \mathbf{r}_{Sp} = {}^{\mathcal{F}_w} [X_{Sp}(t), Y_{Sp}(t), 0]^T. \quad (2)$$

$\{\mathcal{F}_l\}$ is the local reference frame with axes $\{x_l^-, y_l^-, z_l^-\}$ and its origin O_l located at O_{sp} . x_l^- and y_l^- are along the SR's longitudinal and lateral axes. z_l^- is upward and perpendicular to the ground. $\{\mathcal{F}_s\}$ with axes $\{x_s^-, y_s^-, z_s^-\}$ is the shaft reference frame whose origin is at O_s . x_s^- and y_s^- are along the SR's longitudinal and transverse axes. z_s^- is mutually perpendicular to x_s^- and y_s^- by following the right-hand rule.

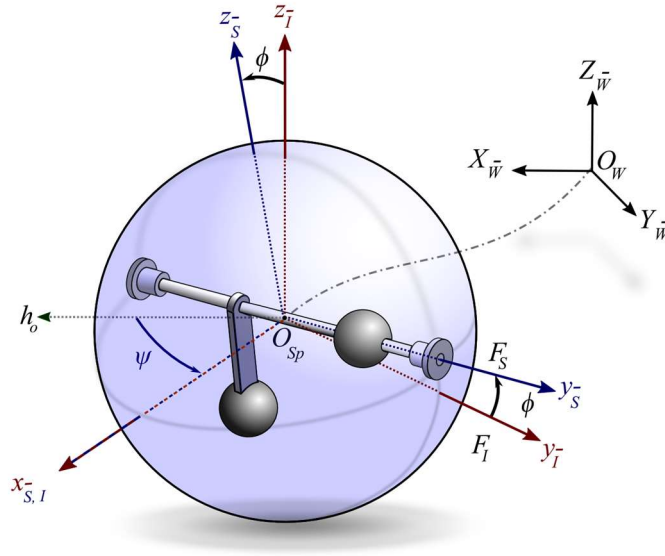


Fig. 3. Reference frames used in the spherical robot kinematics model.

As depicted in Fig. 3, x_l^- and y_l^- are always horizontal i.e. parallel to $X_w^- Y_w^-$ plane and rotated about z_l^- axis by the angle of ψ that is the SR's turning angle about its vertical axis. In other words, the angle between X_w^-

and x_i^- is ψ . Accordingly, $\{\hat{I}, \hat{J}, \hat{K}\}$, $\{\hat{i}, \hat{j}, \hat{k}\}$, and $\{\hat{i}_s, \hat{j}_s, \hat{k}_s\}$ represent unit vectors of $\{\mathcal{F}_w\}$, $\{\mathcal{F}_l\}$, and $\{\mathcal{F}_s\}$ respectively. The next section is dedicated to the derivation of the kinematics and dynamics of Norma.

3. KINEMATICS AND DYNAMICS MODELING OF NORMA

In this section, first, the kinematics equations of the SR's turning maneuver are developed. Then, using Euler-Lagrange method, dynamics equations of motion of the robot are derived.

A. Kinematics and Modeling of Turning Action

Norma's turning action is modeled in Fig. 4. By considering the SR at tilting angle of ϕ , using an imaginary cone with an apex angle of 2ϕ that is purely rolling over the ground. The cone's instantaneous axis of rotation is the imaginary contact line of the cone with the ground, passing through the vertex of the cone, V , and the SR point of contact with the ground C_p . Based on assumption (1) and according to the equal-arc-length rule for rolling without slipping [32] for the cone's base circle, we have:

$$r_c \dot{\theta} = \rho \dot{\psi}, \quad (3)$$

where r_c is cone's base circle's radius, and ρ is the instantaneous radius of curvature of the turning motion that is the distance between the vertex of the cone and the contact point. Considering R as sphere's radius we have:

$$r_c = RC_\phi, \quad (4)$$

$$\rho = -RC_\phi / S_\phi. \quad (5)$$

Where C_\bullet and S_\bullet represent $\cos(\bullet)$ and $\sin(\bullet)$ respectively. Substituting (4) and (5) in (3) results in:

$$\dot{\psi} = -\dot{\theta} S_\phi. \quad (6)$$

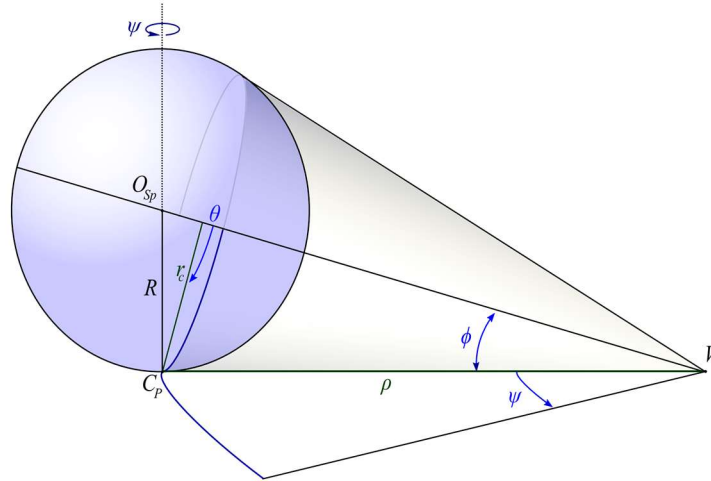


Fig. 4. Rolling cone model of the spherical robot's turning maneuver.

Now, the position vector of the O_{sp} in $\{\mathcal{F}_l\}$ with respect to C_p can be written as:

$${}^{\mathcal{F}_l} \overline{C_p O_{sp}} = R \hat{k}, \quad (7)$$

Also, according to the definition of θ and ϕ , and from (6), the sphere's angular velocity is written as:

$${}^{\mathcal{F}_l} \Omega_{sp} = \dot{\phi} \hat{i} + \dot{\theta} C_\phi \hat{j} - \dot{\theta} S_\phi \hat{k}. \quad (8)$$

Then, the linear velocity vector of O_{sp} can be calculated in $\{\mathcal{F}_l\}$ as the following:

$${}^{\mathcal{F}_I}V_{Sp} = {}^{\mathcal{F}_I}\Omega_{Sp} \times {}^{\mathcal{F}_I}r_{C_pO} = R\dot{\theta}C_\phi\hat{i} - R\dot{\phi}\hat{j}. \quad (9)$$

In ${}^{\mathcal{F}_I}V_{Sp}$, the sphere velocity in z_1^- direction is ${}^{\mathcal{F}_I}w_{Sp} = 0$, so it can be denoted as:

$${}^{\mathcal{F}_I}V_{Sp} = {}^{\mathcal{F}_I}\begin{bmatrix} u_{Sp} \\ v_{Sp} \\ 0 \end{bmatrix}^T. \quad (10)$$

As shown in Fig. 3, transformation matrix from $\{\mathcal{F}_I\}$ to $\{\mathcal{F}_W\}$ is a rotation matrix about z_1^- and angle of ψ as follows:

$$\mathcal{R}_{\mathcal{F}_W\mathcal{F}_I} = \begin{bmatrix} C_\psi & -S_\psi & 0 \\ S_\psi & C_\psi & 0 \\ 0 & 0 & 1 \end{bmatrix}. \quad (11)$$

Therefore, using (9) - (11), one can write the velocity of O_{Sp} in $\{\mathcal{F}_W\}$ as ${}^{\mathcal{F}_W}V_{Sp} = \mathcal{R}_{\mathcal{F}_W\mathcal{F}_I} {}^{\mathcal{F}_I}V_{Sp}$ that results in:

$$\begin{aligned} {}^{\mathcal{F}_W}\dot{X}_{Sp} &= R\dot{\theta}C_\phi C_\psi + R\dot{\phi}S_\psi, \\ {}^{\mathcal{F}_W}\dot{Y}_{Sp} &= R\dot{\theta}C_\phi S_\psi - R\dot{\phi}C_\psi. \end{aligned} \quad (12)$$

So far, the angular velocity of SR about its vertical axis is calculated, and regardless of dynamic states of the elements in the SR, the velocity of the robot is introduced in the local and global reference frames.

B. Motion Dynamics of SR

Using the Euler-Lagrange method, the motion dynamics of the robot is represented as:

$$\frac{d}{dt}\left(\frac{\partial \mathcal{L}}{\partial \dot{q}_i}\right) - \frac{\partial \mathcal{L}}{\partial q_i} = \mathcal{U}_i, \text{ for } i=1,2,3,4, \quad (13)$$

where $q = [\theta, \alpha, \phi, \delta]^T$ is the set of independent generalized coordinates that describe the robot's configuration and $\mathcal{U} = [\mathcal{U}_\theta, \mathcal{U}_\alpha, \mathcal{U}_\phi, \mathcal{U}_\delta]^T$ are external torques and forces that are applied to the corresponding generalized coordinates. \mathcal{L} is the Lagrangian function that can be expressed as:

$$\mathcal{L}(q, \dot{q}) = E^k(q, \dot{q}) - E^p(q), \quad (14)$$

where E^k and E^p denote the total kinetic and potential energies of the robot respectively. In Norma, the gravitational torques cause the sphere to roll with respect to $\{\mathcal{F}_I\}$ and for derivation of E^k and E^p , all vector quantities are calculated in $\{\mathcal{F}_I\}$.

To calculate E^p , since the elevation of the sphere does not vary in $\{\mathcal{F}_I\}$, only the slider and the pendulum of the SR contribute to E^p , whose elevations are derived in the following. In Fig. 1, the pendulum rotation around the shaft is denoted by α in opposite direction to the sphere's rolling rotation, θ . Also, consider the initial direction of the pendulum to be in RSEP. In that case, the difference between the two angles $\alpha - \theta$ measures the angle between the pendulum and its initial direction. So, the position vector ${}^{\mathcal{F}_S}r_p$ of the pendulum bob in $\{\mathcal{F}_S\}$ can be written as follows:

$${}^{\mathcal{F}_S}r_p = LS_{\alpha\theta}\hat{i}_S - L_0\hat{j}_S - LC_{\alpha\theta}\hat{k}_S, \quad (15)$$

where L is the pendulum's length, $S_{\alpha\theta}$ and $C_{\alpha\theta}$ represent $\sin(\alpha - \theta)$ and $\cos(\alpha - \theta)$ respectively. Furthermore, as shown in Fig. 3, $\{\mathcal{F}_S\}$ is resulted from rotation of $\{\mathcal{F}_I\}$ by angle of ϕ about x_1^- . Thus, defining $\mathcal{R}_{\mathcal{F}_I\mathcal{F}_S}$ as:

$$\mathcal{R}_{\mathcal{F}_I\mathcal{F}_S} = \begin{bmatrix} 1 & 0 & 0 \\ 0 & C_\phi & S_\phi \\ 0 & -S_\phi & C_\phi \end{bmatrix}, \quad (16)$$

from (15) and utilizing (16), pendulum in position in $\{\mathcal{F}_I\}$ can be written as follows:

$${}^{\mathcal{F}_I}r_P = \mathcal{R}_{\mathcal{F}_I\mathcal{F}_S} {}^{\mathcal{F}_S}r_P = LS_{\alpha\theta}\hat{i} + (-L_0C_\phi + LC_{\alpha\theta}S_\phi)\hat{j} - (LC_{\alpha\theta}C_\phi + L_0S_\phi)\hat{k}. \quad (17)$$

Based on the definition of δ and δ_0 , position of the slider in $\{\mathcal{F}_S\}$ is:

$${}^{\mathcal{F}_S}r_{Sl} = (\delta + \delta_0)\hat{j}_S, \quad (18)$$

that can be represented in $\{\mathcal{F}_I\}$ as:

$${}^{\mathcal{F}_I}r_{Sl} = \mathcal{R}_{\mathcal{F}_I\mathcal{F}_S} {}^{\mathcal{F}_S}r_{Sl} = (\delta + \delta_0)C_\phi\hat{j} + (\delta + \delta_0)S_\phi\hat{k}. \quad (19)$$

Now, using the pendulum bob and slider positions in (17) and (19) the potential energy of the robot can be written as follows:

$$E^p = m_{sl}g(\delta + \delta_0)S_\phi - m_Pg(LC_{\alpha\theta}C_\phi + L_0S_\phi). \quad (20)$$

In calculation of E^k , kinetic energy of all the SR components, namely the sphere, the pendulum, and the slider, denoted respectively as E_{Sp}^k , E_P^k , and E_{Sl}^k , contribute:

$$E^k = E_{Sp}^k + E_P^k + E_{Sl}^k, \text{ with} \\ E_{Sp}^k = \frac{1}{2}(m_{Sp}\|{}^{\mathcal{F}_I}V_{Sp}\|^2 + {}^{\mathcal{F}_I}\Omega_{Sp}^T I_{Sp} {}^{\mathcal{F}_I}\Omega_{Sp}), E_P^k = \frac{1}{2}(m_P\|{}^{\mathcal{F}_I}V_P\|^2 + {}^{\mathcal{F}_I}\Omega_P^T I_P {}^{\mathcal{F}_I}\Omega_P), \text{ and} \\ E_{Sl}^k = \frac{1}{2}(m_{Sl}\|{}^{\mathcal{F}_I}V_{Sl}\|^2 + {}^{\mathcal{F}_I}\Omega_{Sl}^T I_{Sl} {}^{\mathcal{F}_I}\Omega_{Sl}), \quad (21)$$

where ${}^{\mathcal{F}_I}V$ s and ${}^{\mathcal{F}_I}\Omega$ s are linear velocity and angular velocity vectors of each component. In (21), subscripts Sp , P , and Sl stand for the sphere, pendulum, and the slider respectively. Further, since the sphere shell and the shaft are fixed to each other, they are considered as a single part, Sp , with the total mass of m_{Sp} . I_{Sp} , I_P , and I_{Sl} are moments of inertia matrices of the sphere (with the shaft attached), pendulum, and the slider with respect to $\{\mathcal{F}_I\}$. In the following, linear and angular velocities of all the Norma components are derived to complete the calculation of E^k in (21).

For the sphere, ${}^{\mathcal{F}_I}\Omega_{Sp}$ and ${}^{\mathcal{F}_I}V_{Sp}$ are presented in (8)-(9). For the pendulum, ${}^{\mathcal{F}_I}V_P$ can be written as:

$${}^{\mathcal{F}_I}V_P = V_P^{rel} + {}^{\mathcal{F}_I}V_{O_S} + {}^{\mathcal{F}_I}\Omega_{\mathcal{F}_S} \times {}^{\mathcal{F}_I}r_P, \quad (22)$$

where V_P^{rel} is the relative velocity of the pendulum in $\{\mathcal{F}_I\}$ assuming that $\{\mathcal{F}_S\}$ is stationary. ${}^{\mathcal{F}_I}V_{O_S}$ is the relative linear velocity of the origin of $\{\mathcal{F}_S\}$ in $\{\mathcal{F}_I\}$, and ${}^{\mathcal{F}_I}\Omega_{\mathcal{F}_S}$ is the angular velocity of $\{\mathcal{F}_S\}$ in $\{\mathcal{F}_I\}$. ${}^{\mathcal{F}_I}r_P$ is the position vector of the pendulum that is presented in (15). Calculation steps to derive the terms of equation (22) are presented in the following. The angular velocity of the pendulum in $\{\mathcal{F}_S\}$ is written as follows:

$${}^{\mathcal{F}_S}\Omega_P = (\dot{\theta} - \dot{\alpha})\hat{j}_S. \quad (23)$$

Also, ${}^{\mathcal{F}_S}V$ can be calculated as:

$${}^{\mathcal{F}_S}V_P = {}^{\mathcal{F}_S}\Omega_P \times {}^{\mathcal{F}_S}r_P = L(\dot{\alpha} - \dot{\theta})C_{\alpha\theta}\hat{i}_S + L(\dot{\alpha} - \dot{\theta})S_{\alpha\theta}\hat{k}_S. \quad (24)$$

Then, using (16) and (24), we can write:

$$V_P^{rel} = \mathcal{R}_{\mathcal{F}_I\mathcal{F}_S} {}^{\mathcal{F}_S}V_P = L(\dot{\alpha} - \dot{\theta})C_{\alpha\theta}\hat{i} - L(\dot{\alpha} - \dot{\theta})S_{\alpha\theta}S_\phi\hat{j} + L(\dot{\alpha} - \dot{\theta})S_{\alpha\theta}C_\phi\hat{k}. \quad (25)$$

Knowing ${}^{\mathcal{F}_I}\Omega_{\mathcal{F}_S} = \dot{\phi}\hat{i}$ and using (17) the term ${}^{\mathcal{F}_I}\Omega_{\mathcal{F}_S} \times {}^{\mathcal{F}_I}r_P$ in (22) takes the following form:

$${}^{\mathcal{F}_I}\Omega_{\mathcal{F}_S} \times {}^{\mathcal{F}_I}r_P = (L_0S_\phi + LC_{\alpha\theta}C_\phi\dot{\phi})\hat{j} + (LC_{\alpha\theta}S_\phi\dot{\phi} - L_0C_\phi)\hat{k}. \quad (26)$$

Since O_{Sp} and O_S coincide instantaneously, we have ${}^{\mathcal{F}_I}V_{O_S} = {}^{\mathcal{F}_I}V_{Sp}$ and from (9) we can write:

$${}^{\mathcal{F}_1}V_{O_s} = R\dot{\theta}C_\phi\hat{i} - R\dot{\phi}\hat{j}. \quad (27)$$

Now, combining (25), (26), and (27), (22) can be rewritten as:

$$\begin{aligned} {}^{\mathcal{F}_1}V_P = & \left(R\dot{\theta}C_\phi + L(\dot{\alpha} - \dot{\theta})C_{\alpha\theta} \right)\hat{i} + \left(-L(\dot{\alpha} - \dot{\theta})S_{\alpha\theta}S_\phi + (L_0S_\phi + LC_{\alpha\theta}C_\phi - R)\dot{\phi} \right)\hat{j} \\ & + \left(L(\dot{\alpha} - \dot{\theta})S_{\alpha\theta}C_\phi + (-L_0C_\phi + LC_{\alpha\theta}S_\phi\dot{\phi}) \right)\hat{k}. \end{aligned} \quad (28)$$

Moving on, angular velocity of the pendulum, by utilizing (16) and (23), can be calculated as follows:

$${}^{\mathcal{F}_1}\Omega_P = \mathcal{R}_{\mathcal{F}_1\mathcal{F}_s} {}^{\mathcal{F}_s}\Omega_P = \dot{\phi}\hat{i} + (\dot{\theta} - \dot{\alpha})C_\phi\hat{j} - (\dot{\theta} - \dot{\alpha})S_\phi\hat{k}. \quad (29)$$

Similar to the pendulum, the slider linear velocity is written as:

$${}^{\mathcal{F}_1}V_{Sl} = V_{Sl}^{rel} + {}^{\mathcal{F}_1}V_{O_s} + {}^{\mathcal{F}_1}\Omega_{\mathcal{F}_s} \times {}^{\mathcal{F}_1}r_{Sl}, \quad (30)$$

where V_{Sl}^{rel} is relative velocity of the slider in $\{\mathcal{F}_l\}$ assuming that $\{\mathcal{F}_s\}$ is stationary. Since the motion of the slider is always along the shaft axis, y_s^- , the velocity of the slider in $\{\mathcal{F}_s\}$ is:

$${}^{\mathcal{F}_s}V_{Sl} = \dot{\delta}\hat{j}_s. \quad (31)$$

Then, from (16) and (31), V_{Sl}^{rel} becomes:

$$V_{Sl}^{rel} = \mathcal{R}_{\mathcal{F}_1\mathcal{F}_s} {}^{\mathcal{F}_s}V_{Sl} = \dot{\delta}C_\phi\hat{j} + \dot{\delta}S_\phi\hat{k}. \quad (32)$$

Also, in , knowing that ${}^{\mathcal{F}_1}\Omega_{\mathcal{F}_s} = \dot{\phi}\hat{i}$, from (19), the last term of (30) yields to:

$${}^{\mathcal{F}_1}\Omega_{\mathcal{F}_s} \times {}^{\mathcal{F}_1}r_{Sl} = -(\delta + \delta_0)S_\phi\dot{\phi}\hat{j} + (\delta + \delta_0)C_\phi\dot{\phi}\hat{k}. \quad (33)$$

Thus, by plugging (27), (32), and (33) into (30), ${}^{\mathcal{F}_1}V_{Sl}$ can be rewritten as:

$${}^{\mathcal{F}_1}V_{Sl} = \left(R\dot{\theta}C_\phi \right)\hat{i} + \left(\dot{\delta}C_\phi + (-R - (\delta + \delta_0)S_\phi)\dot{\phi} \right)\hat{j} + \left(\dot{\delta}S_\phi + (\delta + \delta_0)C_\phi\dot{\phi} \right)\hat{k}. \quad (34)$$

Finally, to derive ${}^{\mathcal{F}_1}\Omega_{Sl}$, we have:

$${}^{\mathcal{F}_s}\Omega_{Sl} = \dot{\phi}\hat{i}_s + \dot{\theta}\hat{j}_s, \quad (35)$$

which can be transferred to $\{\mathcal{F}_l\}$ using (16) as follows:

$${}^{\mathcal{F}_1}\Omega_{Sl} = \dot{\phi}\hat{i} + \dot{\theta}C_\phi\hat{j} - \dot{\theta}S_\phi\hat{k}. \quad (36)$$

The next step is deriving the kinetic energy for Norma's components. To from the kinetic energy equation of the sphere, from (8) and (9) we have:

$$E_{Sp}^k = \frac{1}{2}m_{Sp} \left((R\dot{\theta}C_\phi)^2 + (-R\dot{\phi})^2 \right) + \frac{1}{2}I_{Sp}^x\dot{\phi}^2 + \frac{1}{2}I_{Sp}^y(\dot{\theta}C_\phi)^2 + \frac{1}{2}I_{Sp}^z(-\dot{\theta}S_\phi)^2, \quad (37)$$

where I_{Sp}^x , I_{Sp}^y , and I_{Sp}^z are the diagonal elements of I_{Sp} that is the sum of the moments of inertia of the shell and the shaft denoted as I_{Shl} and I_{Shf} respectively. Due to the spherical shape of the shell, I_{Shl} is:

$$I_{Shl} = \text{diag}[I_{Shl}^x, I_{Shl}^y, I_{Shl}^z], \text{ with } I_{Shl}^x = I_{Shl}^y = I_{Shl}^z = \frac{2}{3}m_{Shl}R^2, \quad (38)$$

where, m_{Shl} , I_{Shl}^y , and I_{Shl}^z are moments of inertia of the shell about $\{\mathcal{F}_l\}$ axes, and m_{Shl} is the mass of the shell. Considering the shaft as an oblique rod with length of $2R$, rotated with angle of ϕ about x_l^- , I_{Shf} can be written as:

$$I_{Shf} = \text{diag}[I_{Shf}^x, I_{Shf}^y, I_{Shf}^z], \text{ with } I_{Shf}^x = \frac{1}{3}m_{Shl}R^2, I_{Shf}^y = I_{Shf}^x S_\phi^2, I_{Shf}^z = I_{Shf}^x C_\phi^2, \quad (39)$$

where, I_{Shf}^x , I_{Shf}^y , and I_{Shf}^z are the shaft's moment of inertia about $\{\mathcal{F}_l\}$ axes. Now, from (38) and (39), the moment of inertia of the sphere can be calculated as follows:

$$I_{Sp}^x = I_{Shl} + I_{Shf}^x, I_{Sp}^y = I_{Shl} + I_{Shf}^y S_\phi^2, I_{Sp}^z = I_{Shl} + I_{Shf}^z C_\phi^2, \quad (40)$$

To derive E_P^k , using (23) and (24) we have:

$$E_P^k = \frac{1}{2}m_P \left((R\dot{\theta}C_\phi + L(\dot{\alpha} - \dot{\theta})C_{\alpha\theta})^2 + ((L_0S_\phi + LC_{\alpha\theta}C_\phi - R)\dot{\phi} - L(\dot{\alpha} - \dot{\theta})S_{\alpha\theta}S_\phi)^2 \right. \\ \left. + (L(\dot{\alpha} - \dot{\theta})S_{\alpha\theta}C_\phi + (-L_0C_\phi + LC_{\alpha\theta}S_\phi)\dot{\phi})^2 \right) + \frac{1}{2}I_P^x\dot{\phi}^2 + \frac{1}{2}I_P^y((\dot{\theta} - \dot{\alpha})C_\phi)^2 + \frac{1}{2}I_P^z((\dot{\alpha} - \dot{\theta})S_\phi)^2, \quad (41)$$

in which, I_P^x , I_P^y , and I_P^z are pendulum's moment of inertia about $\{\mathcal{F}_I\}$ axes. Since the pendulum bob is considered to be a point mass, we have:

$$I_P^x = m_P(L_0^2 + (LC_{\alpha\theta})^2), \quad I_P^y = m_P(LC_{\alpha\theta}C_\phi + L_0S_\phi)^2, \quad I_P^z = m_P(L_0C_\phi - LS_\phi)^2. \quad (42)$$

Likewise, using (34) and (35), E_{SI}^k takes the following form:

$$E_{SI}^k = \frac{1}{2}m_{SI} \left((R\dot{\theta}C_\phi)^2 + (\dot{\delta}C_\phi - (R + (\delta + \delta_0)S_\phi)\dot{\phi})^2 + (\dot{\delta}S_\phi + (\delta + \delta_0)C_\phi\dot{\phi})^2 \right) \\ + \frac{1}{2}I_{SI}^x\dot{\phi}^2 + \frac{1}{2}I_{SI}^y(\dot{\theta}C_\phi)^2 + \frac{1}{2}I_{SI}^z(-\dot{\theta}S_\phi)^2, \quad (43)$$

where considering the slider as a point mass, I_{SI} is derived as the following:

$$I_{SI} = \text{diag}[I_{SI}^x \ I_{SI}^y \ I_{SI}^z], \quad \text{with } I_{SI}^x = m_{SI}(\delta + \delta_0)^2, \quad I_{SI}^y = m_{SI}((\delta + \delta_0)S_\phi)^2, \quad I_{SI}^z = m_{SI}((\delta + \delta_0)C_\phi)^2. \quad (44)$$

As the last step, substituting (37), (41), (43), and (20) in (14), and using moments of inertia that are presented in (40),(42), and (44), then, the Lagrange function can be written as:

$$\mathcal{L} = E_{Sp}^k + E_P^k + E_{SI}^k - E^P \\ = \frac{1}{2}m_{Sp} \left((R\dot{\theta}C_\phi)^2 + (-R\dot{\phi})^2 \right) + \frac{1}{2}(I_{Shl} + I_{Shf}^x)\dot{\phi}^2 \\ + \frac{1}{2}(I_{Shl} + I_{Shf}^xS_\phi^2)(\dot{\theta}C_\phi)^2 + \frac{1}{2}(I_{Shl} + I_{Shf}^xC_\phi^2)(-\dot{\theta}S_\phi)^2 \\ + \frac{1}{2}m_P \left((R\dot{\theta}C_\phi + L(\dot{\alpha} - \dot{\theta})C_{\alpha\theta})^2 + ((L_0S_\phi + LC_{\alpha\theta}C_\phi - R)\dot{\phi} - L(\dot{\alpha} - \dot{\theta})S_{\alpha\theta}S_\phi)^2 \right. \\ \left. + (L(\dot{\alpha} - \dot{\theta})S_{\alpha\theta}C_\phi + (-L_0C_\phi + LC_{\alpha\theta}S_\phi)\dot{\phi})^2 + \frac{1}{2}m_P(L_0^2 + (LC_{\alpha\theta})^2)\dot{\phi}^2 \right. \\ \left. + \frac{1}{2}m_P(LC_{\alpha\theta}C_\phi + L_0S_\phi)^2((\dot{\theta} - \dot{\alpha})C_\phi)^2 + \frac{1}{2}m_P(L_0C_\phi - LS_\phi)^2((\dot{\alpha} - \dot{\theta})S_\phi)^2 \right. \\ \left. + \frac{1}{2}m_{SI} \left((R\dot{\theta}C_\phi)^2 + (\dot{\delta}C_\phi - (R + (\delta + \delta_0)S_\phi)\dot{\phi})^2 + (\dot{\delta}S_\phi + (\delta + \delta_0)C_\phi\dot{\phi})^2 \right) \right. \\ \left. + \frac{1}{2}m_{SI}(\delta + \delta_0)^2\dot{\phi}^2 + \frac{1}{2}m_{SI}((\delta + \delta_0)S_\phi)^2(\dot{\theta}C_\phi)^2 + \frac{1}{2}m_{SI}((\delta + \delta_0)C_\phi)^2(-\dot{\theta}S_\phi)^2 \right. \\ \left. - m_{SI}g(\delta + \delta_0)S_\phi + m_Pg(LC_{\alpha\theta}C_\phi + L_0S_\phi) \right). \quad (45)$$

Eventually, using (45) in (13), the equations of motion of Norma can be arranged to take the follow form:

$$M(q)\ddot{q} + C(q,\dot{q})\dot{q} + G(q) = \mathcal{U}, \quad (46)$$

where $M \in \mathbb{R}^{4 \times 4}$ is the inertia matrix, $C \in \mathbb{R}^{4 \times 4}$ is the Coriolis and centripetal matrix, and $G(q) \in \mathbb{R}^{4 \times 1}$ is the vector of gravitational torques and forces. The elements of \mathcal{U} take a zero value when there is a conservative motion in the associated coordinate. Hence, $\mathcal{U}_\theta = 0$, $\mathcal{U}_\alpha = \mathcal{T}$, $\mathcal{U}_\phi = 0$, $\mathcal{U}_\delta = \mathcal{F}$. The element-wise representation of (46) is:

$$\begin{bmatrix} M_{11} & M_{12} & M_{13} & M_{14} \\ M_{21} & M_{22} & M_{23} & M_{24} \\ M_{31} & M_{32} & M_{33} & M_{34} \\ M_{41} & M_{42} & M_{43} & M_{44} \end{bmatrix} \begin{bmatrix} \ddot{\theta} \\ \ddot{\alpha} \\ \ddot{\phi} \\ \ddot{\delta} \end{bmatrix} + \begin{bmatrix} C_{11} & C_{12} & C_{13} & C_{14} \\ C_{21} & C_{22} & C_{23} & C_{24} \\ C_{31} & C_{32} & C_{33} & C_{34} \\ C_{41} & C_{42} & C_{43} & C_{44} \end{bmatrix} \begin{bmatrix} \dot{\theta} \\ \dot{\alpha} \\ \dot{\phi} \\ \dot{\delta} \end{bmatrix} + \begin{bmatrix} G_1 \\ G_2 \\ G_3 \\ G_4 \end{bmatrix} = \begin{bmatrix} \mathcal{T} \\ 0 \\ 0 \\ \mathcal{F} \end{bmatrix}. \quad (47)$$

In appendix A, the calculation steps for deriving the terms and elements in equations (47) have been elaborately presented.

4. PATH PLANNING AND CONTROL OF THE SR

In this section, the path tracking problem of the SR is investigated. First, a kinematics controller is designed that determines the desired values for the rolling angular velocity $\dot{\theta}_d$ and the slider displacement δ_d . Then, a dynamics controller is introduced to govern \mathcal{T} and \mathcal{F} so the above desired values are achieved.

A. Kinematics Control

To make the SR track a desired path, as the first step, a kinematics control scheme based on pure pursuit method [33] is proposed in this subsection. In Fig. 5, consider \mathcal{P} as a two dimensional desired trajectory for the SR represented as ${}^{\mathcal{F}_w}[x_d(t), y_d(t)]^T$, that is assumed to be smooth i.e. $\|{}^{\mathcal{F}_w}[\dot{x}_d, \dot{y}_d]^T\|$ is bounded for $t \geq 0$. It is desired that the location of O_{Sp} in $\{\mathcal{F}_w\}$, ${}^{\mathcal{F}_w}r_{Sp} = {}^{\mathcal{F}_w}[X_{Sp}(t), Y_{Sp}(t)]^T$, converges to \mathcal{P} with a stable error.

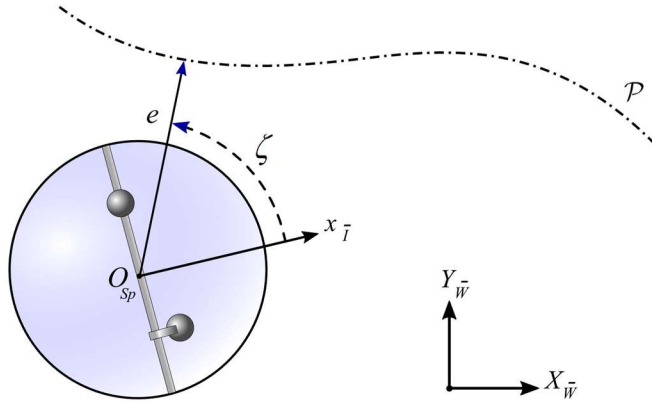


Fig. 5, The kinematics control for the spherical robot.

In Fig.5, let us define the tracking error vector as:

$$e = {}^{\mathcal{F}_w}P_{Sp} - {}^{\mathcal{F}_w}[x_d(t), y_d(t)]^T, \quad (48)$$

and the deviation angle between the SR's heading, ${}^{\mathcal{F}_w}x_t = [\cos(\psi), \sin(\psi)]^T$, and vector e as:

$$\zeta = \angle(e, {}^{\mathcal{F}_w}x_t). \quad (49)$$

The objective of the kinematics control is to send the tracking error e and also the deviation angle ζ to zero. To that end, we design the desired values of the slider displacement and the rolling angular velocity as follows:

$$\delta_d = k_1 \frac{\|e\|}{k_3 + \|e\|} \sin(\zeta), \text{ and} \quad (50)$$

$$\dot{\theta}_d = \frac{1}{R} \|\dot{x}_d, \dot{y}_d\|^T + k_2 \frac{\|e\|}{k_3 + \|e\|} \cos(\zeta). \quad (51)$$

where k_1 , k_2 , and k_3 are design parameters. In the above equations, $\|e\|/(k_3 + \|e\|)$ is used as a normalized error gain to prevent large control efforts at the vicinity of the target point. δ_d is selected to be directly proportional

to $\sin(\zeta)$ as a measure of required tilting to compensate the deviation angle. In the design of $\dot{\theta}_d$, one can easily recognize that $\|[\dot{x}_d, \dot{y}_d]^T\|/R$ is the target's speed translated to the SR rolling velocity, $\dot{\theta}$. Therefore, this speed is chosen as the bias value for $\dot{\theta}_d$. To compensate the magnitude of e , the second term of $\dot{\theta}_d$ uses $\cos(\zeta)$ multiplied with the normalized error gain. $\cos(\zeta)$ is positive or negative when the SR is behind or ahead of the target respectively. Now, that the SR's desired states are determined, the next step is to design a dynamic control scheme to track them.

B. SR Dynamics Control

In this step, a PID-based control scheme is presented for transforming $\dot{\theta}_d$ and δ_d to proper control actions in terms of \mathcal{T} and \mathcal{F} applied to the pendulum and slider respectively. The control block diagram is depicted in Fig.6. As can be seen, two major control loops are designated for the tracking problem. The lower loop controls the slider's displacement. The applied force to the slider has two terms: (1) a force, equal to $gm_{sl}\sin\phi$, against the gravity that is fed forward to prevent the slider from slipping when the SR is tilted, (2) a PID controller's output that is tuned to compensate the slider's displacement error. The upper loop controls the rolling angular velocity $\dot{\theta}$. To that end, first, an inner loop is designed to control the pendulum angle, $\alpha - \theta$. Then, an outer loop is tuned to compensate the angular velocity error $\dot{\theta}_d - \dot{\theta}$ by governing the pendulum angle.

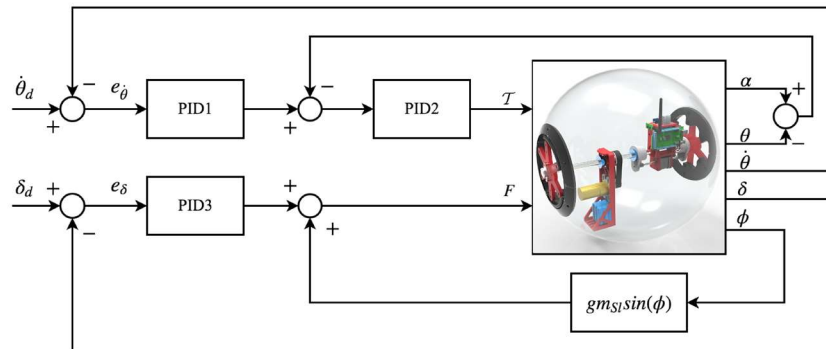


Fig. 6. The schematic of PID controller structure for the spherical robot.

5. EXPERIMENTAL AND SIMULATION RESULTS

A. Experimental Setup

As it is depicted in Fig. 7, the experimental setup is designed and implemented on a Linux based system. Three Raspberry Pis (Model Zero W) are mounted inside the SR. Two Raspberry Pis are utilized for controlling the DC and stepper motors while the third one is used to acquire the tilting angle data of the SR. The tilting angle is measured using ST LSM303D Inertial Measurement Unit (IMU). Python socket library is in charge of data transferring between the Raspberry Pis and the PC where the main Python script on the PC is defined as the server and each Raspberry Pi is defined as a client. Clients and the server communicate through a common Wi-Fi network.

A single ceiling mounted wide-angle camera with 120° field of view is used for the purpose of localization to obtain the position and heading direction of the robot. Robot's spherical shell is marked with red and blue colors side by side into two halves and the color of the test field is selected to be dark green. Python OpenCV library is implemented to perform the image processing task. First, the center location of each one of the two

color regions, i.e. $C_{blue}=[x_{blue}, y_{blue}]$ and $C_{red}=[x_{red}, y_{red}]$, is determined in Hue Saturation Value (HSV) color space using blob detection method. Then, to form error and deviation angle vectors based on (48) and (49), the position and orientation of the SR are calculated as the following:

$$\begin{aligned} x_{Sp} &= (x_{blue} + x_{red})/2, \text{ and } y_{Sp} = (y_{blue} + y_{red})/2, \\ x_{heading} &= y_{blue} - y_{red}, \text{ and } y_{heading} = x_{red} - x_{blue}. \end{aligned} \quad (52)$$

In order to achieve real time tracking, the resolution of the captured frames is selected to be 640×480 pixels at a frame rate of 30 frames per second (fps).

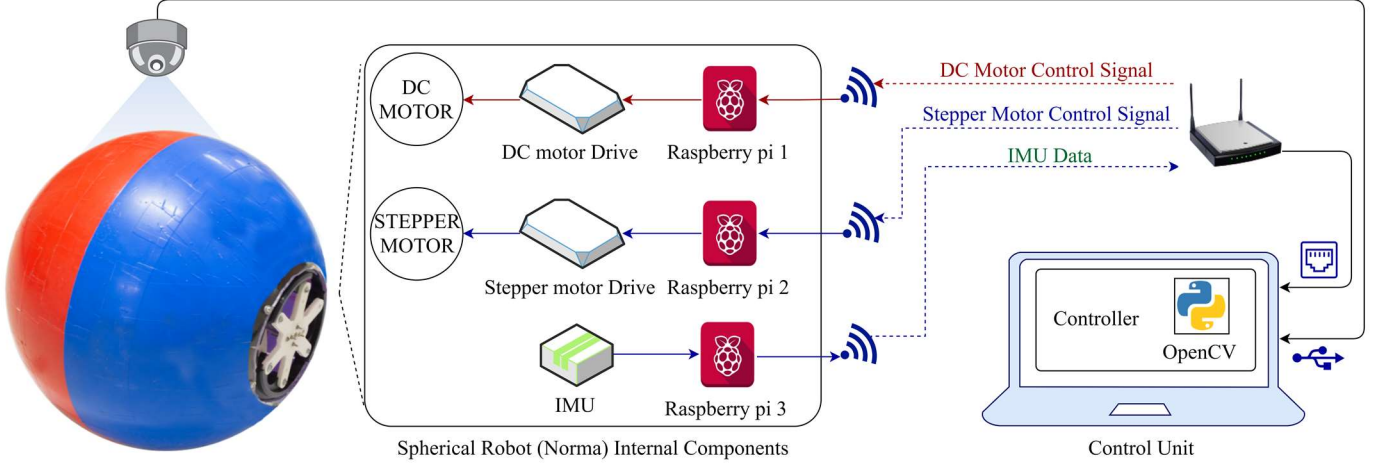


Fig. 7. The setup utilized for experimental results' acquisition.

B. Simulation and Experimental Results.

In this subsection, the presented mathematical model of Norma is evaluated against experimental results using the control scheme proposed in the section 5. The SR parameters are chosen based on the actual robot as follows: $R=0.2\text{m}$, $L=0.15\text{m}$, $L_0=0.10\text{m}$, $\delta_0=0.1\text{m}$, $m_{Sp}=3\text{kg}$, $m_{shf}=m_p=m_{sl}=0.5\text{kg}$, $g=9.81\text{m/s}^2$, $k_1=0.1$, $k_2=-0.1$, and $k_3=5$. Also, the PID controllers in Fig. 6 are tuned using values given in Table 1, which were obtained by trial-and-error.

Table 1: Numerical values of the PID parameters.

	K_p	K_I	K_D
<i>PID1</i>	1	0	0
<i>PID2</i>	10	7	3
<i>PID3</i>	15	3	10

The simulations are carried out, where the desired trajectory \mathcal{P} is chosen to be:

$${}^{\mathcal{F}_w} [X_d, Y_d] = [2S_{0.01t}, 1.5S_{0.02t}] \text{ and } {}^{\mathcal{F}_w} [X_{Sp}(0), Y_{Sp}(0)] = [0, 0]. \quad (53)$$

Fig. 8 shows a sequence of images captured by the camera during the experiments. Blue and red color regions of the robot's body can be seen in the pictures as well as detected centers, C_{blue} and C_{red} that are drawn automatically by the program as small yellow circles. The infinity symbol shaped path presented in (53) has been added to the pictures graphically to show the desired trajectory.

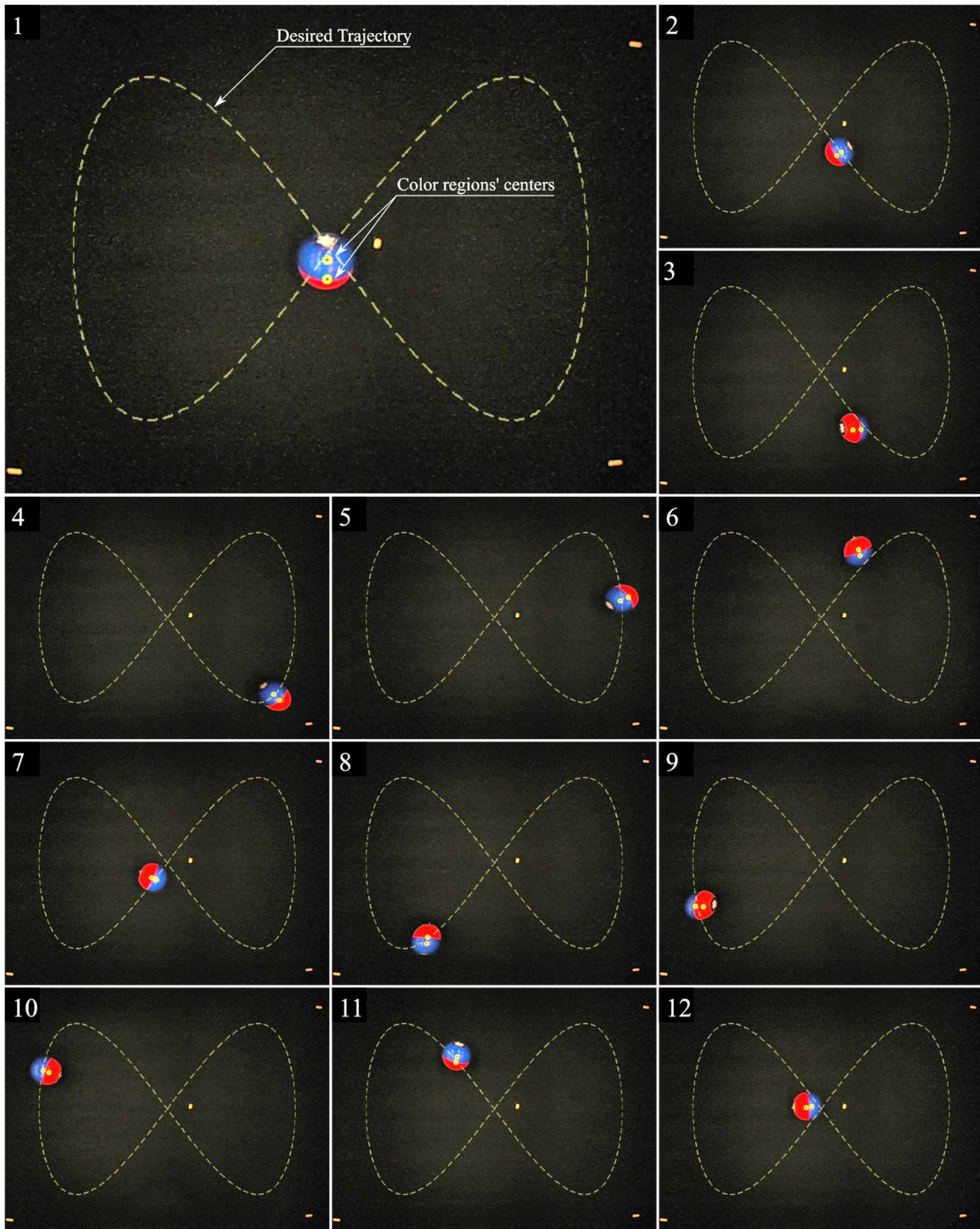


Fig. 8. SR trajectory in XY plane during infinity shape maneuver captured by the camera.

The trajectory tracking performance of Norma in XY plane is presented in Fig. 9. Fig. 10 compares the SR's closed loop time response of the mathematical model and the positions measured in experiments. It can be observed that the SR can track the desired path successfully, and the tracking error converges to the vicinity of zero in a relatively short amount of time. The control actions governed by the PID controllers are given in Fig.11. Finally, Fig. 12 illustrates the tilting angle calculated during the analysis and measured as experimental result.

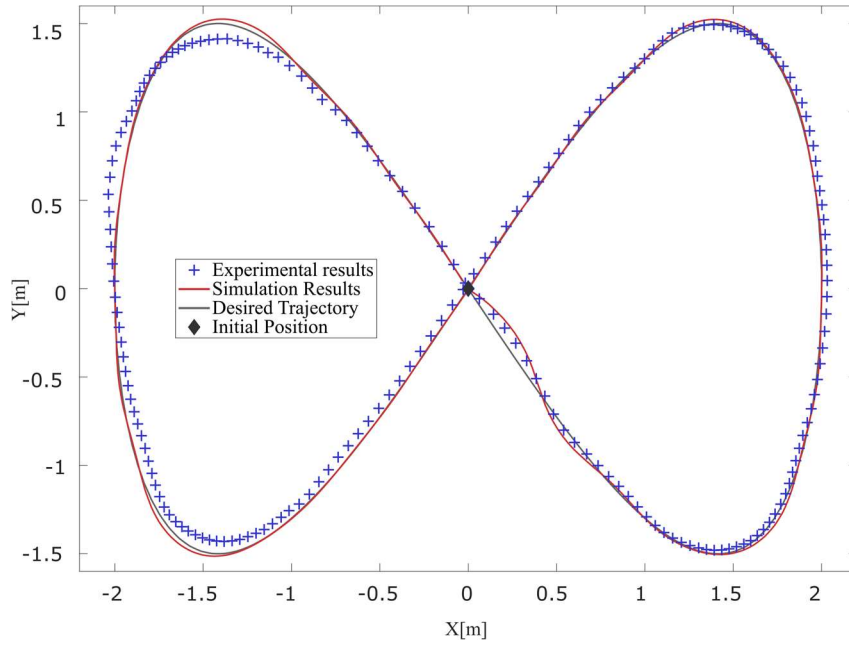


Fig. 9. Robot's desired, actual and simulation trajectories in XY plane.

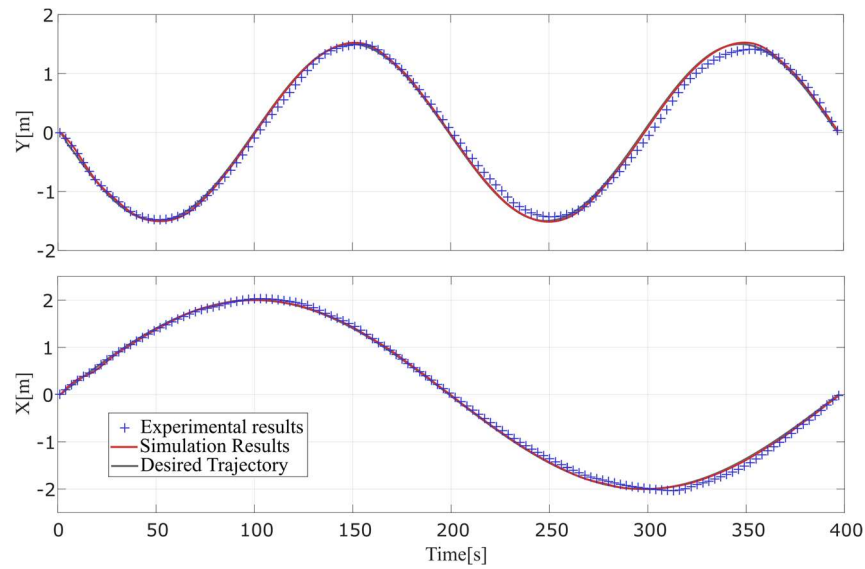


Fig. 10. SR trajectory in X and Y directions versus time.

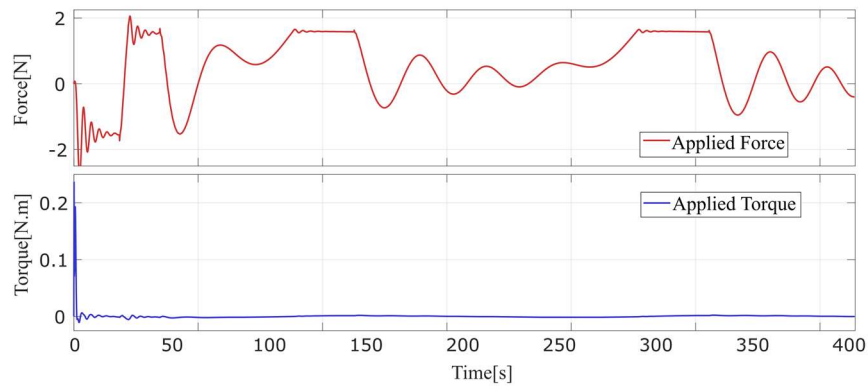


Fig. 11. Control actions governed by the controllers.

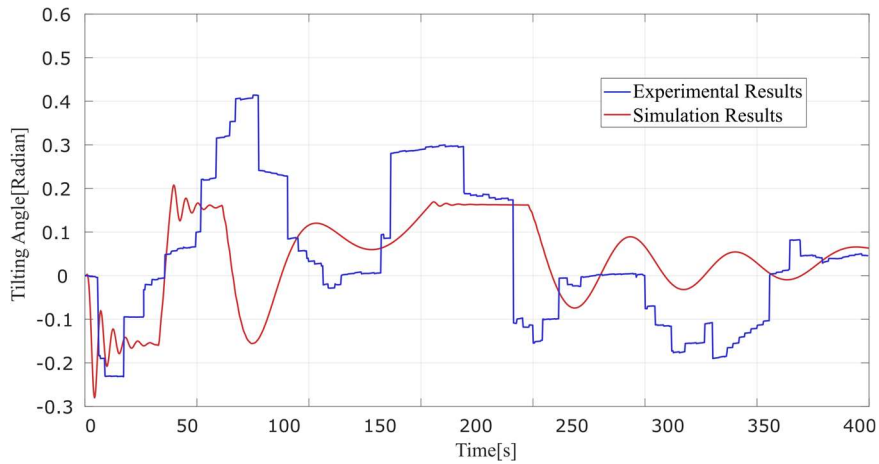


Fig. 12. Robot's Tilting angle.

C. Comparison

Although, it has been tried to involve as minimum simplifications as possible in the modeling of Norma, there are inevitable differences between the behavior of the mathematical model and the actual robot, and it is worthwhile to discuss some of them here. The mathematical model has an ideal point contact with the surface. Conversely, in the actual robot, the nature of the robot's contact point with the ground is not an ideal point due to a slight deformation of the SR's shell at the contact point and/or penetration of the robot into soft floor materials. Also, the robot shows asymmetrical behavior due to the accuracy of the fabrication process. For example, a certain amount of slider displacement along the negative and positive directions leads to two different tilting angles. Generally, the mathematical model shows higher agility compared to the actual robot. The actual robot usually needs slightly higher tilting angle to perform a similar maneuver compared to the mathematical model and it needs more time to reach a desired value imposed from the controller. It can be mainly due to the deformation of the shell at the contact point and the resistance of the test field material to rolling and tilting actions of the robot specially in relatively low $\dot{\theta}$ and δ values.

6. CONCLUSION AND FUTURE WORKS

Dynamics of spherical robots has intrinsic complexities, which poses challenges to accurately model them. In this paper, we presented the structure, fabrication, mathematical modeling, and experimental results of Norma, a novel 2-DOF SR. It has been tried to avoid simplifications in developing the Lagrangian-based model of the SR in order to acquire accurate equations of motion. We also presented a kinematics and dynamics control scheme to track a desired trajectory by the robot and verified its performance by the mathematical and experimental results.

The primary focus of this paper is to introduce the dynamics of the proposed SR. In another research paper [4], kinematics of Norma has been investigated on 3D terrains. One more step is to study the control problem of the derived dynamics in details. Finally, incorporating results of these studies, dynamics modeling, control, and 3D kinematics of Norma, the objective of this research project is to introduce a general model for the proposed SR.

APPENDIX A

This appendix aims to show calculation steps that have been carried out in order to derive terms of the SR equations of motion presented in (47). Based on the Lagrange-Euler method, first we calculate the $\partial\mathcal{L}/\partial\dot{q}_i$ term for each generalized coordinate in q . Then, we collect the resulting expression in the following format:

$$\frac{\partial\mathcal{L}}{\partial\dot{q}_i} = \sum_{j=1}^4 M_{ij} \dot{q}_j = M_{i1}\dot{\theta} + M_{i2}\dot{\alpha} + M_{i3}\dot{\phi} + M_{i4}\dot{\delta}. \quad (\text{A.1})$$

For $q_1 = \theta$, partial derivative of \mathcal{L} with respect to $\dot{q}_1 = \dot{\theta}$ can be written in the form of:

$$\frac{\partial\mathcal{L}}{\partial\dot{\theta}} = M_{11}\dot{\theta} + M_{12}\dot{\alpha} + M_{13}\dot{\phi} + M_{14}\dot{\delta}, \quad (\text{A.2})$$

where, M_{11} through M_{14} can be calculated as:

$$\begin{aligned} M_{11} = & L^2 m_P C_{\alpha\theta}^2 (1 + C_\phi^4) - 2LL_0 m_P C_\phi S_\phi^3 + 2Lm_P C_{\alpha\theta} C_\phi (L_0 C_\phi^2 S_\phi - R) + L^2 m_P S_\phi^2 (S_{\alpha\theta}^2 + S_\phi^2) \\ & + C_\phi^2 \left(I_{Shl} + (m_P + m_{Sl} + m_{Sp}) R^2 + L^2 m_P S_{\alpha\theta}^2 + \left(I_{Shf}^x + 2(L_0^2 m_P + m_{Sl} (\delta_0 + \delta)^2) \right) S_\phi^2 \right), \end{aligned} \quad (\text{A.3})$$

$$\begin{aligned} M_{12} = & -m_P \left(L^2 C_{\alpha\theta}^2 (1 + C_\phi^4) - 2LL_0 C_\phi S_\phi^3 + LC_{\alpha\theta} C_\phi (2L_0 C_\phi^2 S_\phi - R) + L^2 S_\phi^2 (S_{\alpha\theta}^2 + S_\phi^2) \right) \\ & + C_\phi^2 \left(L^2 S_{\alpha\theta}^2 + 2L_0^2 S_\phi^2 \right), \end{aligned} \quad (\text{A.4})$$

$$M_{13} = Lm_P S_{\alpha\theta} (L_0 - RS_\phi), \quad (\text{A.5})$$

$$M_{14} = 0. \quad (\text{A.6})$$

For $q_2 = \alpha$, $\partial\mathcal{L}/\partial\dot{\alpha}$ will be:

$$\frac{\partial\mathcal{L}}{\partial\dot{\alpha}} = M_{21}\dot{\theta} + M_{22}\dot{\alpha} + M_{23}\dot{\phi} + M_{24}\dot{\delta}, \quad (\text{A.7})$$

where terms M_{21} through M_{24} are as follows:

$$M_{21} = M_{12}, \quad (\text{A.8})$$

$$M_{22} = m_P \left(L^2 C_{\alpha\theta}^2 + L^2 C_\phi^2 S_{\alpha\theta}^2 + S_\phi^2 \left((L_0 C_\phi - LS_\phi)^2 + L^2 S_{\alpha\theta}^2 \right) + C_\phi^2 (LC_{\alpha\theta} C_\phi + L_0 S_\phi)^2 \right), \quad (\text{A.9})$$

$$M_{23} = -Lm_P S_{\alpha\theta} (L_0 - RS_\phi), \quad (\text{A.10})$$

$$M_{24} = 0. \quad (\text{A.11})$$

For $q_3 = \phi$ we have:

$$\frac{\partial\mathcal{L}}{\partial\dot{\phi}} = M_{31}\dot{\theta} + M_{32}\dot{\alpha} + M_{33}\dot{\phi} + M_{34}\dot{\delta}, \quad (\text{A.12})$$

where, M_{31} through M_{34} are as the following:

$$M_{31} = M_{13}, \quad (\text{A.13})$$

$$M_{32} = M_{23}, \quad (\text{A.14})$$

$$\begin{aligned} M_{33} = & I_{Shl} + I_{Shf}^x + 2m_{Sl} (\delta_0 + \delta)^2 + (m_P + m_{Sl} + m_{Sp}) R^2 + m_P \left(L^2 (1 + C_{2\alpha\theta}) + 2L_0^2 - 2RLC_{\alpha\theta} C_\phi \right) \\ & + 2R(m_{Sl} (\delta_0 + \delta) - L_0 m_P) S_\phi, \end{aligned} \quad (\text{A.15})$$

$$M_{34} = -m_{Sl} RC_\phi. \quad (\text{A.16})$$

Finally, for $q_4 = \delta$, $\partial\mathcal{L}/\partial\dot{\delta}$ is written as:

$$\frac{\partial\mathcal{L}}{\partial\dot{\delta}} = M_{41}\dot{\theta} + M_{42}\dot{\alpha} + M_{43}\dot{\phi} + M_{44}\dot{\delta}, \quad (\text{A.17})$$

with

$$M_{41} = M_{14}, \quad (\text{A.18})$$

$$M_{42} = M_{24}, \quad (\text{A.19})$$

$$M_{43} = M_{34}, \text{ and} \quad (\text{A.20})$$

$$M_{44} = m_{sl}. \quad (\text{A.21})$$

The next step is to derive the terms of $C(q, \dot{q})$ and $G(q)$ to form the equation (46). It can be shown that there is not a unique arrangement for the elements in C . For controller design applications, it is preferred to form C such that the matrix

$$N(q, \dot{q}) = \dot{M}(q, \dot{q}) - 2C(q, \dot{q}), \quad (\text{A.22})$$

be a skew-symmetric i.e. $N^T = -N$. To that end, the C elements are determined as:

$$C_{ij} = \sum_{k=1}^4 c_{kji} \dot{q}_k, \quad (\text{A.23})$$

where,

$$c_{kji} = \frac{1}{2} \left(\frac{\partial M_{ij}}{\partial q_k} + \frac{\partial M_{ik}}{\partial q_j} - \frac{\partial M_{kj}}{\partial q_i} \right). \quad (\text{A.24})$$

c_{kji} are the so-called Christoffel [34] symbols of the first kind. Therefore, using (A.23) and (A.24), for $q_1 = \theta$, terms of C_{11} through C_{14} are calculated as:

$$\begin{aligned} C_{11} = & C_\phi \left(Lm_P (\dot{\alpha} - \dot{\theta}) S_{\alpha\theta} \left(R - C_\phi^2 (LC_{\alpha\theta} C_\phi + L_0 S_\phi) \right) m_{sl} (\delta_0 + \delta) \dot{\delta} S_\phi S_{2\phi} \right) + \frac{1}{8} \dot{\phi} \left(LL_0 m_P C_{(\alpha\theta)/2}^2 C_{4\phi} \right. \\ & + 8Lm_P \left(-L_0 C_{2\phi} S_{(\alpha\theta)/2}^2 + RC_{\alpha\theta} S_\phi \right) - 2S_{2\phi} \left(2I_{Shl} + 2(m_P + m_{sl} + m_{sp}) R^2 + L^2 m_P (C_{2\alpha\theta} - 1) \right) \\ & \left. + S_{4\phi} \left(2I_{Shf}^x + 4L_0^2 m_P + 4m_{sl} (\delta_0 + \delta)^2 - L^2 m_P (3 + C_{2\alpha\theta}) \right) \right), \end{aligned} \quad (\text{A.25})$$

$$\begin{aligned} C_{12} = & Lm_P C_\phi (\dot{\alpha} - \dot{\theta}) S_{\alpha\theta} \left(LC_{\alpha\theta} C_\phi^3 + L_0 C_\phi^2 S_\phi - R \right) + \frac{1}{4} m_P \dot{\phi} \left(8L^2 C_{\alpha\theta}^2 C_\phi^3 S_\phi \right. \\ & \left. - 2LC_{\alpha\theta} \left(L_0 (C_{2\phi} + C_{4\phi}) + RS_\phi \right) \right. \\ & \left. + 4LS_\phi \left(L_0 S_{3\phi} - LC_\phi \right) + S_{4\phi} \left(L^2 - 2L_0^2 \right) \right), \end{aligned} \quad (\text{A.26})$$

$$\begin{aligned} C_{13} = & \frac{1}{8} \left(8LL_0 m_P C_{(\alpha\theta)/2}^2 C_{4\phi} (\dot{\theta} - \dot{\alpha}) + 8LL_0 m_P C_{2\phi} (\dot{\alpha} - \dot{\theta}) S_{(\alpha\theta)/2}^2 \right. \\ & \left. - 8L^2 m_P \dot{\phi} S_{2\alpha\theta} - 4Lm_P RC_{2\alpha\theta} (\dot{\alpha} - 2\dot{\theta}) S_\phi \right. \\ & \left. + 2 \left(\left(L^2 m_P (1 - C_{2\alpha\theta}) - 2I_{Shl} - 2(m_P + m_{sl} + m_{sp}) R^2 \right) \dot{\theta} - 2L^2 m_P \dot{\alpha} S_{\alpha\theta}^2 \right) S_{2\phi} + \left(m_P \dot{\alpha} \left(L^2 (3 + C_{2\alpha\theta}) - 4L_0^2 \right) \right. \right. \\ & \left. \left. + \left(2I_{Shl} - 3L^2 m_P + 4L_0^2 m_P + 4m_{sl} (\delta_0 + \delta)^2 - L^2 m_P C_{2\alpha\theta} \right) \dot{\theta} \right) S_{4\phi} \right), \end{aligned} \quad (\text{A.27})$$

$$C_{14} = 2m_{sl} \dot{\theta} (\delta_0 + \delta) C_\phi^2 S_\phi^2. \quad (\text{A.28})$$

Using the same method, for $q_2 = \alpha$ we can calculate C_{21} through C_{24} as the following:

$$\begin{aligned} C_{21} = & Lm_P C_\phi^3 (\dot{\alpha} - \dot{\theta}) S_{\alpha\theta} \left(LC_{\alpha\theta} C_\phi + L_0 S_\phi \right) + \frac{1}{4} m_P \dot{\phi} \left(8L^2 C_{\alpha\theta}^2 C_\phi^3 S_\phi - 2LC_{\alpha\theta} \left(L_0 (C_{2\phi} + C_{4\phi}) + RS_\phi \right) \right. \\ & \left. + 4LS_\phi \left(L_0 S_{3\phi} - LC_\phi \right) + \left(L^2 - 2L_0^2 \right) S_{4\phi} \right), \end{aligned} \quad (\text{A.29})$$

$$\begin{aligned} C_{22} = & -Lm_P C_\phi^3 (\dot{\alpha} - \dot{\theta}) S_{\alpha\theta} \left(LC_{\alpha\theta} C_\phi + L_0 S_\phi \right) - \frac{1}{4} m_P \dot{\phi} \left(-4LC_\phi \left(L_0 C_{\alpha\theta} C_{3\phi} + LS_\phi - 2LC_{\alpha\theta}^2 C_\phi^2 S_\phi \right) \right. \\ & \left. + 4LL_0 S_\phi S_{3\phi} + \left(L^2 - 2L_0^2 \right) S_{4\phi} \right), \end{aligned} \quad (\text{A.30})$$

$$\begin{aligned}
C_{23} = & \frac{1}{8}m_p \left(8LL_0C_{\alpha\theta}^2C_{4\phi}(\dot{\alpha}-\dot{\theta}) + 8LL_0C_{2\phi}(\dot{\theta}-\dot{\alpha})S_{\alpha\theta}^2 + 8L^2\dot{\phi}S_{2\alpha\theta} - 4LRC_{\alpha\theta}\dot{\theta}S_{\phi} \right. \\
& + 4L^2(\dot{\alpha}-\dot{\theta})S_{\alpha\theta}^2S_{2\phi} \\
& \left. - (L^2(3+C_{2\alpha\theta})-4L_0^2)(\dot{\alpha}-\dot{\theta})S_{4\phi} \right),
\end{aligned} \tag{A.31}$$

$$C_{24} = 0. \tag{A.32}$$

Next, for $q_3 = \phi$, C_{31} through C_{34} are as follows:

$$\begin{aligned}
C_{31} = & Lm_p \left(2LC_{\alpha\theta} - RC_{\phi} \right) \dot{\phi}S_{\alpha\theta} + \frac{1}{4}m_p\dot{\alpha} \left(2L(-4LC_{\alpha\theta}^2C_{\phi}^3S_{\phi} + C_{\alpha\theta}(L_0(2+C_{2\phi}+C_{4\phi})-RS_{\phi})) + LS_{2\phi} \right. \\
& \left. - 2L_0S_{\phi}S_{3\phi} \right) - (L^2-2L_0^2)S_{4\phi} + \frac{1}{8}\dot{\theta} \left(-8LL_0m_p \left(C_{\alpha\theta} + C_{\alpha\theta/2}^2C_{4\phi} \right) + 8LL_0m_pC_{2\phi}S_{\alpha\theta/2}^2 \right. \\
& \left. + 2(2I_{Shl} + L^2m_p(C_{2\alpha\theta}-1) + 2R^2(m_p+m_{Sl}+m_{Sp}))S_{2\phi} - (2I_{Shf}^x - 3L^2m_p + 4L_0^2m_p + 4m_{Sl}(\delta+\delta_0))^2 \right. \\
& \left. - L^2m_pC_{2\alpha\theta} \right) S_{4\phi} \Big),
\end{aligned} \tag{A.33}$$

$$\begin{aligned}
C_{32} = & \frac{1}{8}m_p \left(8LL_0 \left(C_{\alpha\theta/2}^2C_{4\phi}(\dot{\theta}-\dot{\alpha}) + 8LL_0C_{2\phi}(\dot{\alpha}-\dot{\theta})S_{\alpha\theta/2}^2 + 8LR\dot{\phi}C_{\phi}S_{\alpha\theta} \right. \right. \\
& \left. \left. + 8LC_{\alpha\theta}(L_0\dot{\theta}-L_0\dot{\alpha}-2L\dot{\phi}S_{\alpha\theta}) \right. \right. \\
& \left. \left. + 4LRC_{\alpha\theta}(2\dot{\alpha}-\dot{\theta})S_{\phi} + 4L^2(\dot{\theta}-\dot{\alpha})S_{\alpha\theta}^2S_{2\phi} + (L^2(C_{2\alpha\theta}+3)-4L_0^2)(\dot{\alpha}-\dot{\theta})S_{4\phi} \right) \right),
\end{aligned} \tag{A.34}$$

$$\begin{aligned}
C_{33} = & Lm_p \left(-2LC_{\alpha\theta} + RC_{\phi} \right) (\dot{\alpha}-\dot{\theta})S_{\alpha\theta} + m_{Sl}\dot{\delta} \left(2(\delta_0+\delta) + RsS_{\phi} \right) \\
& + R\dot{\phi} \left((m_{Sl}(\delta_0+\delta) - L_0m_p)C_{\phi} + Lm_pC_{\alpha\theta}S_{\phi} \right),
\end{aligned} \tag{A.35}$$

$$C_{34} = m_{Sl}\dot{\phi} \left(2(\delta_0+\delta) + RS_{\phi} \right). \tag{A.36}$$

Finally, for $q_4 = \delta$, C_{41} through C_{44} are:

$$C_{41} = -2m_{Sl}(\delta_0+\delta)C_{\phi}^2\dot{\theta}S_{\phi}^2, \tag{A.37}$$

$$C_{42} = 0, \tag{A.38}$$

$$C_{43} = -2m_{Sl}(\delta_0+\delta)\dot{\phi}, \tag{A.39}$$

$$C_{44} = 0. \tag{A.40}$$

The last step is to calculate $G(q)$, using the following equation,

$$G_i(q) = \frac{\partial E^p}{\partial q_i}. \tag{A.41}$$

for $q_1 = \theta$ through $q_4 = \delta$ we have:

$$G_1 = -gLm_pC_{\phi}S_{\alpha\theta}, \tag{A.42}$$

$$G_2 = gLm_pC_{\phi}S_{\alpha\theta}, \tag{A.43}$$

$$G_3 = g \left((m_{Sl}(\delta_0+\delta) - L_0m_p)C_{\phi} + Lm_pC_{\alpha\theta}S_{\phi} \right), \tag{A.44}$$

$$G_4 = gm_{Sl}S_{\phi}. \tag{A.45}$$

By substituting calculated terms of matrix $M(q)$, $C(q,\dot{q})$, and $G(q)$ in (47), the dynamics model for the presented spherical robot is complete.

REFERENCES

- [1] W.-H. Chen, C.-P. Chen, J.-S. Tsai, J. Yang, and P.-C. Lin, "Design and implementation of a ball-driven omnidirectional spherical robot," *Mechanism and Machine Theory*, vol. 68, pp. 35-48, 2013/10/01/ 2013.
- [2] R. Chase and A. Pandya, "A Review of Active Mechanical Driving Principles of Spherical Robots," vol. 1, no. 1, p. 3, 2012.
- [3] V. A. J. P. Crossley, Pa, "A literature review on the design of spherical rolling robots," pp. 1-6, 2006.
- [4] S. Moazami, H. Zargarzadeh, and S. Palanki, "Kinematics of Spherical Robots Rolling Over 3D Terrains," *arXiv preprint arXiv:1906.05228*, 2019.
- [5] M. Seeman, M. Broxvall, A. Saffiotti, and P. Wide, "An autonomous spherical robot for security tasks," in *Computational Intelligence for Homeland Security and Personal Safety, Proceedings of the 2006 IEEE International Conference on*, 2006, pp. 51-55: IEEE.
- [6] M. Li, S. Guo, H. Hirata, and H. Ishihara, "Design and performance evaluation of an amphibious spherical robot," *Robotics and Autonomous Systems*, vol. 64, pp. 21-34, 2015.
- [7] Z. Qiang, L. Zengbo, and C. Yao, "A back-stepping based trajectory tracking controller for a non-chained nonholonomic spherical robot," *Chinese Journal of Aeronautics*, vol. 21, no. 5, pp. 472-480, 2008.
- [8] J. D. Hernández, J. Barrientos, J. del Cerro, A. Barrientos, and D. Sanz, "Moisture measurement in crops using spherical robots," vol. 40, no. 1, pp. 59-66, 2013.
- [9] F. Michaud, T. Salter, A. Duquette, and J.-F. Laplante, "Perspectives on mobile robots as tools for child development and pediatric rehabilitation," *Assistive Technology*, vol. 19, no. 1, pp. 21-36, 2007.
- [10] F. Michaud and S. Caron, "Roball, the rolling robot," *Autonomous robots*, vol. 12, no. 2, pp. 211-222, 2002.
- [11] Z. Qiang, C. Yao, and Y. Caixia, "Design, analysis and experiments of an omni-directional spherical robot," in *2011 IEEE International Conference on Robotics and Automation*, 2011, pp. 4921-4926.
- [12] L. Wang and B. Zhao, "Dynamic modeling and control strategy for turning in place motion of a two-coaxial pendulums driven spherical inspector based on stick-slip principle," *Mechanism and Machine Theory*, vol. 83, pp. 69-80, 2015/01/01/ 2015.
- [13] Y. Cai, Q. Zhan, and X. Xi, "Path tracking control of a spherical mobile robot," *Mechanism and Machine Theory*, vol. 51, pp. 58-73, 2012.
- [14] M. Taheri Andani, Z. Ramezani, S. Moazami, J. Cao, M. M. Arefi, and H. Zargarzadeh, "Observer-Based Sliding Mode Control for Path Tracking of a Spherical Robot %J Complexity," vol. 2018, p. 15, 2018, Art. no. 3129398.
- [15] B. P. DeJong, E. Karadogan, K. Yelamarthi, and J. Hasbany, "Design and Analysis of a Four-Pendulum Omnidirectional Spherical Robot," *Journal of Intelligent & Robotic Systems*, vol. 86, no. 1, pp. 3-15, 2017/04/01 2017.
- [16] T. J. Ylikorpi, A. J. Halme, and P. J. Forsman, "Dynamic modeling and obstacle-crossing capability of flexible pendulum-driven ball-shaped robots," *Robotics and Autonomous Systems*, vol. 87, pp. 269-280, 2017/01/01/ 2017.
- [17] Q. Jia, H. Sun, and D. Liu, "Analysis of Actuation for a Spherical Robot," in *2008 IEEE Conference on Robotics, Automation and Mechatronics*, 2008, pp. 266-271.
- [18] F. Tomik, S. Nudehi, L. L. Flynn, and R. Mukherjee, "Design, Fabrication and Control of Spherobot: A Spherical Mobile Robot," *Journal of Intelligent & Robotic Systems*, vol. 67, no. 2, pp. 117-131, 2012/07/01 2012.
- [19] V. A. Joshi, R. N. Banavar, and R. Hippalgaonkar, "Design and analysis of a spherical mobile robot," *Mechanism and Machine Theory*, vol. 45, no. 2, pp. 130-136, 2010/02/01/ 2010.
- [20] M. R. Azizi and D. Naderi, "Dynamic modeling and trajectory planning for a mobile spherical robot with a 3Dof inner mechanism," *Mechanism and Machine Theory*, vol. 64, pp. 251-261, 2013/06/01/ 2013.
- [21] P. Mojabi, "Introducing glory: A novel strategy for an omnidirectional spherical rolling robot," *Journal of Dynamic Systems, Measurement, and Control*, vol. 126, no. 3, pp. 678-683, 2004.
- [22] Q. Zhan, Y. Cai, and C. Yan, "Design, analysis and experiments of an omni-directional spherical robot," in *Robotics and Automation (ICRA), 2011 IEEE International Conference on*, 2011, pp. 4921-4926: IEEE.
- [23] J. Alves and J. Dias, "Design and control of a spherical mobile robot," *Proceedings of the Institution of Mechanical Engineers, Part I: Journal of Systems and Control Engineering*, vol. 217, no. 6, pp. 457-467, 2003.
- [24] V. Kaznov and M. Seeman, "Outdoor navigation with a spherical amphibious robot," in *Intelligent Robots and Systems (IROS), 2010 IEEE/RSJ International Conference on*, 2010, pp. 5113-5118: IEEE.
- [25] J.-C. Yoon, S.-S. Ahn, and Y.-J. Lee, "Spherical robot with new type of two-pendulum driving mechanism," in *Intelligent Engineering Systems (INES), 2011 15th IEEE International Conference on*, 2011, pp. 275-279: IEEE.

- [26] B. Zhao, M. Li, H. Yu, H. Hu, and L. Sun, "Dynamics and motion control of a two pendulums driven spherical robot," in *Intelligent Robots and Systems (IROS), 2010 IEEE/RSJ International Conference on*, 2010, pp. 147-153: IEEE.
- [27] M. Nagai, "Control system for a spherical robot," Master, Department of Automation and System Technology, Lulea University of Technology, 2008.
- [28] E. Kayacan, Z. Y. Bayraktaroglu, and W. Saeys, "Modeling and control of a spherical rolling robot: a decoupled dynamics approach," *Robotica*, vol. 30, no. 4, pp. 671-680, 2012.
- [29] M. Roozegar and M. J. Mahjoob, "Modelling and control of a non-holonomic pendulum-driven spherical robot moving on an inclined plane: simulation and experimental results," *IET Control Theory & Applications*, vol. 11, no. 4, pp. 541-549, 2016.
- [30] M. Roozegar, M. Ayati, and M. J. Mahjoob, "Mathematical modelling and control of a nonholonomic spherical robot on a variable-slope inclined plane using terminal sliding mode control," *Nonlinear Dynamics*, journal article vol. 90, no. 2, pp. 971-981, October 01 2017.
- [31] S. Gajbhiye and R. N. Banavar, "The Euler-Poincaré equations for a spherical robot actuated by a pendulum," *IFAC Proceedings Volumes*, vol. 45, no. 19, pp. 72-77, 2012.
- [32] J. H. Ginsberg, *Advanced engineering dynamics*. Cambridge University Press, 1998.
- [33] P. Corke, *Robotics, Vision and Control: Fundamental Algorithms In MATLAB® Second, Completely Revised*. Springer, 2017.
- [34] K. M. Lynch, "Modern Robotics-Mechanics, Planning, and Control: Video supplements and software," 2017.